

ON THE GRAIN-MODIFIED MAGNETIC DIFFUSIVITIES IN PROTOPLANETARY DISKS

RUI XU^{1,2}, XUE-NING BAI³

¹ Department of Astrophysical Sciences, Princeton University, Princeton, NJ 08544; ruix@princeton.edu

² Yuanpei College, Peking University, Beijing, 100871, China and

³ Institute for Theory and Computation, Harvard-Smithsonian Center for Astrophysics, 60 Garden St., MS-51, Cambridge, MA, 02138; xbai@cfa.harvard.edu

Draft version November 24, 2015

ABSTRACT

Weakly ionized protoplanetary disks (PPDs) are subject to non-ideal-magnetohydrodynamic (MHD) effects including Ohmic resistivity, the Hall effect and ambipolar diffusion (AD), and the resulting magnetic diffusivities (η_O , η_H and η_A) largely control the disk gas dynamics. The presence of grains not only strongly reduces disk ionization fraction, but also modify the scalings of η_H and η_A with magnetic field strength. We derive analytically asymptotic expressions of η_H and η_A in both strong and weak field limits and show that towards strong field, η_H can change sign (at a threshold field strength B_{th}), mimicking a flip of field polarity, and AD is substantially reduced. Applying to PPDs, we find that when small ~ 0.1 (0.01) μm grains are sufficiently abundant [mass ratio ~ 0.01 (10^{-4})], η_H can change sign up to $\sim 2 - 3$ scale heights above midplane at modest field strength (plasma $\beta \sim 100$) over a wide range of disk radii. Reduction of AD is also substantial towards the AD dominated outer disk and may activate the magneto-rotational instability. We further perform local non-ideal MHD simulations of the inner disk (within 10 AU) and show that with sufficiently abundant small grains, magnetic field amplification due to the Hall-shear instability saturates at very low level near the threshold field strength B_{th} . Together with previous studies, we conclude by discussing the grain-abundance-dependent phenomenology of PPD gas dynamics.

Subject headings: accretion, accretion disks — magnetohydrodynamics — planetary systems: protoplanetary disks

1. INTRODUCTION

Gas dynamics of the weakly ionized protoplanetary disks (PPDs) is to a large extent controlled by its coupling with magnetic fields, described by non-ideal magnetohydrodynamic (MHD) effects, including Ohmic resistivity, the Hall effect and ambipolar diffusion (AD). The three effects dominate in different regions of PPDs, and affect the gas dynamics in different ways. A constant theme of PPD research has been to estimate the strength of magnetic diffusivities, and study their consequences to gas dynamics, especially on the level of turbulence and efficiency of angular momentum transport (see [Turner et al. 2014](#) for recent review).

The strength of magnetic diffusivities largely depends on gas density ρ , level of ionization, and magnetic field strength B . In the absence of grains, the Ohmic, Hall and ambipolar diffusivities can be expressed in particularly simple form ([Salmeron & Wardle 2003](#))

$$\eta_O = \eta_e, \quad \eta_H = \frac{cB}{4\pi en_e}, \quad \eta_A = \frac{B^2}{4\pi\gamma_i\rho\rho_i}, \quad (1)$$

where $\eta_e \propto (n/n_e)$ is resistivity due to electrons, n_e , n are the electron and neutral number densities, and ρ_i is the ion density.

These expressions are complicated by the presence of dust grains. On the one hand, grains can substantially reduce the level of ionization, and hence boosting all three magnetic diffusivities proportionally. On the other hand, grains carry charge and result in much more complex dependence of diffusivities on magnetic field strength (e.g.,

see [Wardle 2007](#) and [Bai 2014a](#)), yet such complex dependence has not been systematically explored.

As an initial effort, [Bai \(2011b\)](#) (hereafter B11) considered the limit when grains are tiny ($\sim\text{nm}$ sized PAHs) so that the conductivity of charged grains is similar to ions. He showed that when tiny grains are the dominant charge carrier, Hall diffusivity diminishes and AD is substantially reduced in the strong field limit, which may be important in the outer region of PPDs.

In this paper, we extend the work of B11 to more general situations with more typical grain sizes (sub-micron to micron) relevant to PPDs. We focus on the disk interior (rather than surface) where grains are likely the dominant charge carrier, and are mostly singly charged, and systematically explore how magnetic diffusivities depend on field strength. We hope to provide researchers a useful guidance on modeling non-ideal MHD effects from ionization chemistry, which has been fruitful in the recent years (e.g., [Turner et al. 2007](#); [Bai & Stone 2013](#); [Bai 2013, 2014b, 2015](#); [Lesur et al. 2014](#); [Gressel et al. 2015](#); [Simon et al. 2015](#)).

This work is also motivated by the recent advances in understanding the gas dynamics of the Hall effect, where the Hall-shear instability may substantially amplify the midplane field strength in the inner region of PPDs ([Kunz 2008](#); [Lesur et al. 2014](#); [Bai 2014b](#)) when the background field is aligned with disk rotation. With strong field amplification, we discuss whether grain-modified diffusivities can feedback to PPD gas dynamics.

We present our simplified model in Section 2, with application to PPDs discussed in Section 3. We perform

MHD simulations of the inner disk and discuss the results in Section 4. In Section 5, we summarize and conclude.

2. A SIMPLIFIED MODEL FOR GRAIN-MODIFIED DIFFUSIVITIES

In weakly ionized gas, the general expressions for the three magnetic diffusivities are (Wardle 2007; Bai 2011a)

$$\begin{aligned}\eta_O &= \frac{c^2}{4\pi} \frac{1}{\sigma_O}, \quad \eta_H = \frac{c^2}{4\pi} \frac{\sigma_H}{\sigma_H^2 + \sigma_P^2}, \\ \eta_A &= \frac{c^2}{4\pi} \frac{\sigma_P}{\sigma_H^2 + \sigma_P^2} - \eta_O,\end{aligned}\quad (2)$$

where $\sigma_O, \sigma_H, \sigma_P$ are Ohmic, Hall and Pederson conductivities, defined as

$$\begin{aligned}\sigma_O &= \frac{ec}{B} \sum_j n_j |Z_j| \beta_j, \\ \sigma_H &= \frac{ec}{B} \sum_j \frac{n_j Z_j}{1 + \beta_j^2}, \\ \sigma_P &= \frac{ec}{B} \sum_j \frac{n_j |Z_j| \beta_j}{1 + \beta_j^2},\end{aligned}\quad (3)$$

where summation goes over all charged species j , with $n_j, Z_j e$ being the number density and charge of individual charged species. The Hall parameter β_j is given by

$$\beta_j = \frac{|Z_j| e B}{m_j c} \frac{1}{\gamma_j \rho}, \quad (4)$$

which describes the ratio between the gyro-frequency of the charged species and its collision frequency with the neutrals, where $\gamma_j \equiv \langle \sigma v \rangle_j / (\mu_n + m_j)$, with $\langle \sigma v \rangle_j$ being rate coefficient for collisional momentum transfer with the neutrals. The charged species j is strongly coupled to the neutrals if $\beta_j \ll 1$ (weak field), and it is strongly coupled to magnetic fields when $\beta_j \gg 1$ (strong field). The values of $\langle \sigma v \rangle_j$ for electron, ion and grain can be found in Equation (14)-(16) of (Bai 2011a, 2014a), giving Hall parameter

$$\begin{aligned}\beta_e &\approx 2.1 (B/n_{15}) \min [1, T_{100}^{-1/2}], \\ \beta_i &\approx 3.3 \times 10^{-3} (B/n_{15}), \\ \beta_g &\approx (B/n_{15}) \min [3.2 \times 10^{-3} |Z_g|^{-1}, 10^{-9} a_1^{-2} T_{100}^{-1/2}]\end{aligned}\quad (5)$$

where B is magnetic field measured in Gauss, $n_{15} = n_H/10^{15} \text{cm}^{-3}$, Z_g is grain charge, a_1 is grain size in μm , disk temperature $T_{100} = T/100 \text{K}$. Clearly, $\beta_e \gg \beta_i$, and unless grain size is tiny ($a \lesssim \text{nm}$), $\beta_i \gg \beta_g$.

As long as ion mass is much larger than neutral mass, different ion species have their Hall parameters very close to β_i quoted above, and can be treated as a single species. In the interior of PPDs where ionization level is low, chemistry calculations show that (small) grains are largely singly charged until the ionization fraction exceeds grain abundance towards disk surface (e.g., Figure 6 of Wardle 2007 and Figure 1 of Bai 2011a). We also assume single-sized grains for simplicity, which is typically adopted in PPD chemistry calculations. While a grain

size distribution is expected in reality, we expect a single-size treatment to capture and better clarify the essence of their effects. Therefore, we consider only four types of charged species: electrons, ions, and positive/negative charged grains, whose number densities are represented by $n_e, n_i, n_{\text{gr}}^+$ and n_{gr}^- .

Under these conditions, the Hall and Pederson conductivities read

$$\begin{aligned}\sigma_H &= \frac{-1}{1 + \beta_e^2} + \frac{n_i}{n_e} \frac{1}{1 + \beta_i^2} + \frac{n_{\text{gr}}^+ - n_{\text{gr}}^-}{n_e} \frac{1}{1 + \beta_g^2}, \\ \sigma_P &= \frac{\beta_e}{1 + \beta_e^2} + \frac{n_i}{n_e} \frac{\beta_i}{1 + \beta_i^2} + \frac{n_{\text{gr}}^+ + n_{\text{gr}}^-}{n_e} \frac{\beta_g}{1 + \beta_g^2}.\end{aligned}\quad (6)$$

Hereafter, we omit the prefactor $en_e c/B$ in conductivities and $cB/4\pi en_e$ in diffusivities so as to make them dimensionless. The grain-free diffusivities (1) corresponds to $\eta_O = 1/\beta_e$, $\eta_H = 1$ and $\eta_A = \beta_i$, and hence the conventional Ohmic regime applies in weak field with $\beta_e < 1$, AD regime applies in strong field $\beta_i > 1$, and the Hall dominated regime lies in between. For brevity, we further define $n_{\text{gr}}^\pm \equiv n_{\text{gr}}^+ + n_{\text{gr}}^-$.

Charge neutrality guarantees that only three of the four number densities are independent. With additional normalization by n_e , only two of them serve as independent model parameters. We find it useful to choose the two ratios $n_i/n_e, n_{\text{gr}}^\pm/n_e$ as model variables. Without grains, their values are obviously 1 and 0, while when grains become important charge carriers, $n_i \gg n_e$, and $n_{\text{gr}}^\pm > n_i$.

The Hall parameters $\beta_{e,i,g} \propto B$ can be considered as a proxy for magnetic field strength. According to (5), we fix $\beta_i = 10^{-3} \beta_e$ in our calculations. The ratio $\beta_g/\beta_i \propto a^{-2}$ reflects grain size and defines our last (third) model parameter. For $0.1 \mu m$ sized grains, $\beta_g \sim 10^{-4} \beta_i$, and only for $a \sim 10^{-3} \mu m$ we have $\beta_i \sim \beta_g$.

2.1. Asymptotic Relations

We are mainly interested in reducing (6) to sufficiently simple and intuitive expressions. Ohmic resistivity is the most straightforward and can be written as

$$\eta_O = \frac{1}{\beta_e (1 + \theta_1 + \theta_2)}, \quad (7)$$

where we have defined

$$\theta_1 = \frac{n_i}{n_e} \frac{\beta_i}{\beta_e}, \quad \theta_2 = \frac{n_{\text{gr}}^\pm}{n_e} \frac{\beta_g}{\beta_e}. \quad (8)$$

In general, Ohmic resistivity results from electron conductivity. Contributions from the ions and grains become significant ($\theta_{1,2} \gtrsim 1$) only when $n_i/n_e > \beta_e/\beta_i \approx 1000$ and $n_{\text{gr}}^\pm/n_e \gtrsim \beta_e/\beta_g$, both requiring grain charge density to be overwhelmingly dominant.

Calculations of the Hall and ambipolar diffusivities involve much more complex algebra, and sufficiently simple expressions can only be obtained in asymptotic regimes. In the weak field regime (equivalently, Ohmic dominated regime) where $\beta_g \lesssim \beta_i \ll \beta_e \ll 1$, we Taylor expand the expressions for σ_H, σ_P in equation (6) and keep the

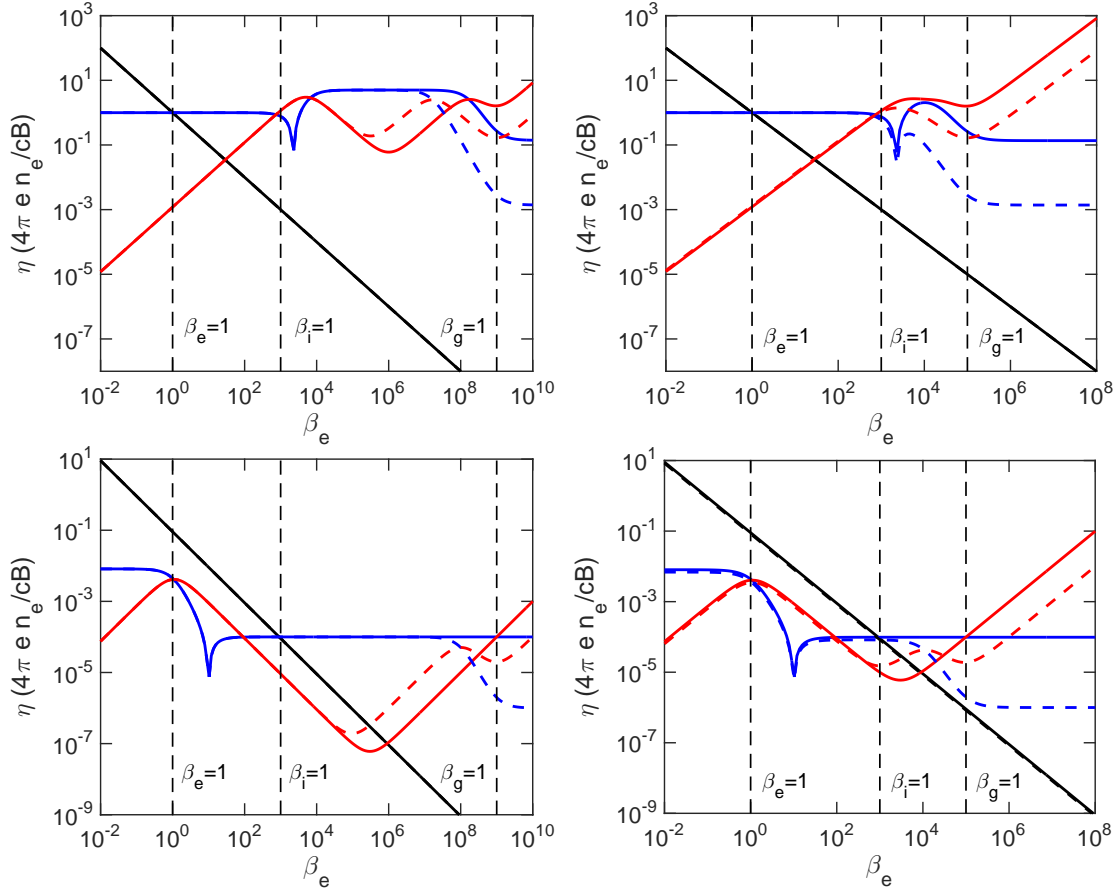


FIG. 1.— Dimensionless Ohmic (black), Hall (blue), and the ambipolar (red) diffusivities as a function of magnetic field strength (manifested as the electron Hall parameter β_e) under various representative parameters. We set $n_i/n_e = 1.2$ and 10^4 in the top and bottom panels, respectively. On the left two panels, we have $\beta_g/\beta_i = 10^{-6}$ (μm sized grain), while in right two panels we have $\beta_g/\beta_i = 10^{-2}$ ($\sim 0.01\mu\text{m}$ sized grain). In each panel, solid lines correspond to $(n_{gr}^+ + n_{gr}^-)/n_i = 1$, while the dashed lines correspond to $(n_{gr}^+ + n_{gr}^-)/n_i = 10$.

leading order terms¹. The results are

$$\sigma_H \approx \beta_e^2, \quad \sigma_P \approx \beta_e[(1 + \theta_1 + \theta_2) - \beta_e^2]. \quad (9)$$

Substituting them to Equation (2), we obtain

$$\eta_H \approx \frac{1}{(1 + \theta_1 + \theta_2)^2}, \quad (10)$$

$$\eta_A \approx \frac{\beta_e(\theta_1 + \theta_2)}{(1 + \theta_1 + \theta_2)^3} = \beta_i \frac{n_i + n_{gr}^\pm(\beta_g/\beta_i)}{n_e(1 + \theta_1 + \theta_2)^3}.$$

These expressions reduces exactly to Equation (15) of B11 ($\beta_g = \beta_i$) by replacing $\theta_1 + \theta_2$ by his θ , and replacing $n_i + n_{gr}^\pm(\beta_g/\beta_i)$ by his $\bar{n} \equiv n_i + n_{gr}^\pm$. As already discussed there, ambipolar diffusivity is enhanced by the presence of charged grains, and the Hall diffusivity can be modestly reduced when $\theta_{1,2} \gtrsim 1$.

In the strong field limit where $1 \ll \beta_g \lesssim \beta_i \ll \beta_e$, we

¹ We have also assumed $n_i/n_e \ll 10^6$, or $\beta_i\theta_1 \ll \beta_e$, which is almost always the case from chemistry calculations.

can reduce the Hall and Pederson conductivities to

$$\sigma_H \approx \frac{\theta_1\beta_e}{\beta_i} \left[\frac{1}{\beta_i^2} - \frac{1}{\beta_g^2} \right] + \frac{1}{\beta_g^2}, \quad (11)$$

$$\sigma_P \approx \beta_e \left[\frac{\theta_1}{\beta_i^2} + \frac{\theta_2}{\beta_g^2} \right].$$

The corresponding Hall and ambipolar diffusivities are

$$\eta_H \approx \frac{[\theta_1\beta_e(\beta_g^2 - \beta_i^2) + \beta_i^3] \beta_i\beta_g^2}{\beta_e^2(\beta_g^2\theta_1 + \beta_i^2\theta_2)^2}, \quad (12)$$

$$\eta_A \approx \frac{\beta_i^2\beta_g^2}{\beta_e(\theta_1\beta_g^2 + \theta_2\beta_i^2)}.$$

In the tiny grain limit of $\beta_g = \beta_i$, these relatively complex expressions can be further reduced to

$$\eta_H \approx \frac{\beta_i^2}{\beta_e^2\theta^2} = \left(\frac{n_e}{\bar{n}} \right)^2, \quad (13)$$

$$\eta_A \approx \frac{(\theta_1 + \theta_2)\beta_i^6}{\beta_e\beta_i^4(\theta_1 + \theta_2)^2} = \frac{\beta_in_e}{\bar{n}},$$

which agree exactly with equation (16) of B11.

From Equation (12), we see that in the strong field regime, η_H becomes negative when

$$\theta_1 \beta_e (\beta_g^2 - \beta_i^2) + \beta_i^3 < 0, \text{ or } \beta_g^2 < \beta_i^2 (1 - \frac{n_e}{n_i}). \quad (14)$$

In general, the sign of η_H depends on the relative mass (mobility) between the positive and negative charge carrier. In the absence of grains, with electrons much more mobile than ions, η_H is positive. In the presence of tiny grains with $\beta_g = \beta_i$ as considered by B11, charged grains are as mobile as normal ions. Therefore, negative charge carriers are still effectively more mobile due to the presence of electrons, and hence $\eta_H \geq 0$. Relation (14) states that, as long as grains are not too small (i.e. well above nanometer size so that $\beta_g \ll \beta_i$), η_H can become negative whenever there are more ions than electrons. In other words, there are more negatively charged grains than positively ones, and hence negative charge carriers are effectively less mobile. We will see in Section 3 that $n_i > n_e$ almost always holds from ionization chemistry calculations in PPDs. The main practical question then is whether disk magnetic field can reach the level such that η_H changes sign. We therefore define B_{th} as the threshold field strength beyond which η_H changes sign, and this is a main quantity of interest that we study in the rest of the paper.

2.2. Representative Cases

In Figure 1, we show the dimensionless Ohmic, Hall and the ambipolar diffusivities as a function of magnetic field strength (characterized by the electron Hall parameter), covering most of the parameter space relevant for grain size $a \gtrsim 0.01 \mu\text{m}$ (see figure caption). We first confirm that $\eta_H \propto B$ and $\eta_A \propto B^2$ holds both in weak ($\beta_e \ll 1$) and strong ($\beta_g \gg 1$) field regimes as expected. In between, we see that both η_H and η_A exhibit complex variations with B , where η_H changes sign in all cases, and η_A is reduced in steps compared with the B^2 scaling.

Top two panels of Figure 1 correspond to cases where grains are modestly important charge carrier, giving n_i/n_e not far from order unity. We see that for field strength with $\beta_i < 1$, η_H and η_A behave normally as in conventional Ohmic and Hall regimes. Sign change of η_H and reduction of η_A are both achieved towards stronger field (in the conventional AD regime) with $\beta_i > 1$ (and $\beta_g < 1$).

On the other hand, in the bottom two panels, assuming grains are the dominant charge carriers such that $n_i/n_e \gg 1$, we see that magnetic diffusivities behaves qualitatively differently. First, the threshold field strength B_{th} for η_H to change sign is much weaker, close to $\beta_e = 1$. Similarly, reduction of η_A starts right from $\beta_e = 1$. Secondly, Ohmic resistivity dominates all the way through the conventional Hall-regime ($\beta_e > 1$, $\beta_i < 1$), while the Hall effect dominates only in much stronger field ($\beta_i > 1$ and $\beta_g < 1$), which is in the conventional AD-dominated regime. AD dominates only when the field is much stronger with $\beta_g > 1$.

Overall, we see that the ratio n_i/n_e largely controls the dependence of η_H and η_A on magnetic field strength, especially towards weaker field ($\beta_i \lesssim 1$). Other parameters (grain size and n_{gr}^\pm/n_i) mainly affect diffusivity behaviors

towards strong field with $\beta_i > 1$, leading to complex dependence before reaching the asymptotic regime (12) at $\beta_g > 1$, and trend can be identified by comparing the left and right panels of Figure 1.

3. APPLICATION TO PROTOPLANETARY DISKS: IONIZATION CHEMISTRY

To test our analytical results, we conduct ionization-recombination chemistry calculation using a complex reaction network developed in Bai & Goodman (2009) and Bai (2011a) that followed from Ilgner & Nelson (2006). There are 175 gas-phase species and over two thousands gas phase reactions extracted from the latest version of the UMIST database (McElroy et al. 2013). The rate coefficients in the data base are given as a function of temperature. One change from our previous chemistry calculations is that when gas temperature lies out of the stated range of validity, we still use the given formula as if it remained valid (whereas originally we computed the coefficients using upper or lower bound of valid temperature range). For inner disk temperatures ($\sim 100 - 300\text{K}$), about 10% of the reactions are affected, majority of which are neutral-neutral reactions, and/or reactions with large activation energy. In the latter case, our original approach tends to significantly overestimate the reaction rates at lower temperatures. Also, for many of these reactions, we note that the rate coefficients listed in the KIDA chemical database generally have different valid temperature ranges with similar coefficients. This change does not affect the level of ionization in the presence of grains (but leads to higher ionization fraction in the grain-free case), while the composition of ion species is affected.

We include a single grain population with maximum grain charge of ± 2 , with fiducial choices of grain size $a = 0.1 \mu\text{m}$ and dust-to-gas mass ratio of $f = 10^{-2}$. Although such grain size and abundance are likely exaggerated considering that substantial grain growth must have occurred in PPDs (e.g., Birnstiel et al. 2010), they are the best to illustrate the effects that we discuss in this paper. Given that large uncertainties remain in our understandings of grain size distribution in PPDs (e.g., D'Alessio et al. 2006), we also consider a few other combinations of grain sizes and abundances to study parameter dependence. Note that for chemical purposes, we are only concerned with the abundance of sub-micron sized grains, which is the most relevant to ionization and charging. We adopt the minimum-mass solar nebular (MMSN) disk model that is vertically isothermal with standard cosmic-ray and X-ray ionization prescriptions as described in Bai (2011a), together with a constant ionization rate of $7 \times 10^{-19} \text{ s}^{-1}$ as a proxy for radioactive decay (the exact value matters little).

The relative importance of non-ideal MHD effects in PPDs is conveniently described by the dimensionless Elsasser numbers, defined as

$$\Lambda \equiv \frac{v_A^2}{\eta_O \Omega_K}, \quad \chi \equiv \frac{v_A^2}{\eta_H \Omega_K}, \quad Am \equiv \frac{v_A^2}{\eta_A \Omega_K}, \quad (15)$$

where $v_A^2 = B^2/4\pi\rho$ is the Alfvén speed, Ω_K is disk angular frequency. Non-ideal MHD effects become dominant when the (absolute value of) respective Elsasser numbers becomes smaller than order unity. Note that in our

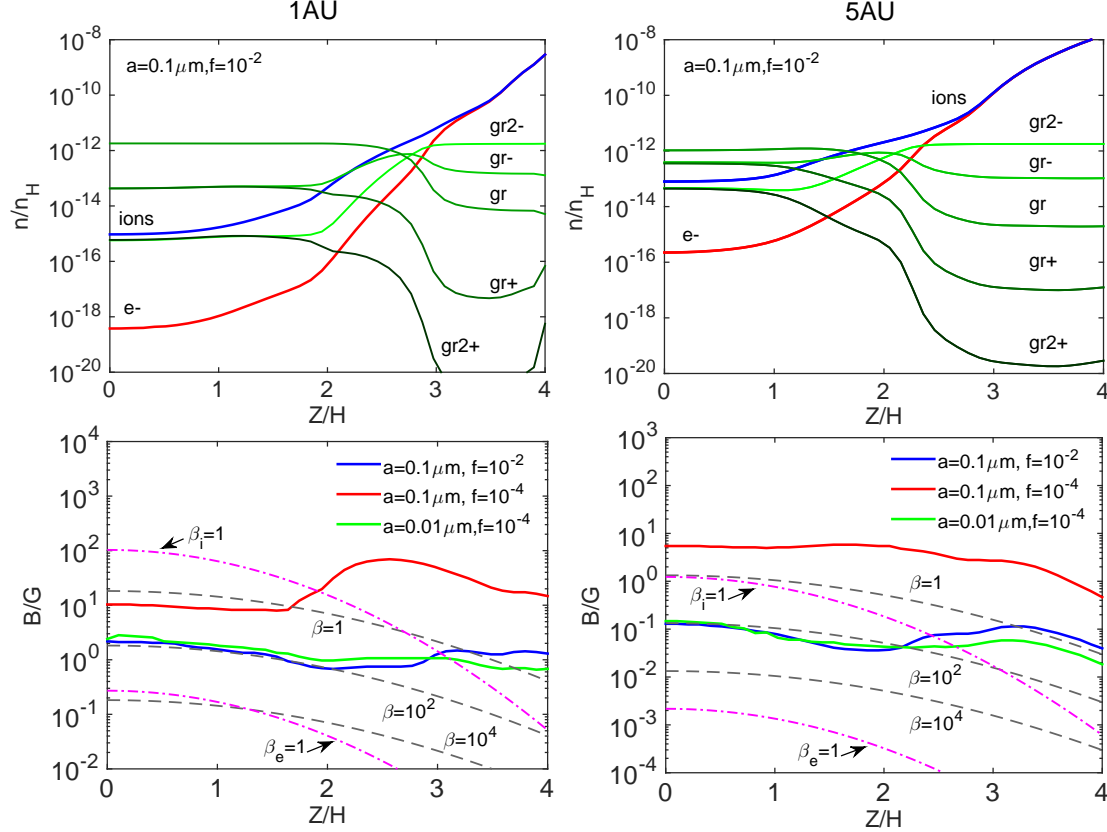


FIG. 2.— Results from ionization chemistry calculations at 1 AU (left) and 5 AU (right). Top panels: abundance of all charged species as a function of height z above disk midplane (normalized to disk scale height H), where $grn(+/-)$ denote positively/negatively charged grains with grain charge n , and the red/blue lines represent abundances of electrons/all ions. Bottom panels: solid lines show threshold field strength B_{th} (beyond which η_H changes sign, in Gauss, see legend) as a function of z based on the chemistry calculations in the top panels. Also shown are the field strengths that correspond to plasma $\beta = 1, 100$ and 10^4 (grey), as well as field strengths that give electron/ion Hall parameters $\beta_e = 1$ and $\beta_i = 1$ (pink). Three combinations of grain size a and dust-to-gas mass ratios f are considered in the bottom panels, as marked in legend, while the top panels correspond to the $a = 0.1\mu m$ and $f = 10^{-2}$ case.

definition, χ will change sign when η_H becomes negative.

3.1. Threshold Field Strength in PPDs

In Figure 2, we show the vertical profile of charged species abundance at 1 AU and 5 AU using fiducial grain size ($a = 0.1\mu m$) and mass ratio ($f = 10^{-2}$) in the top two panels. We see that grains are the dominant charge carriers within $\sim 2 - 3$ disk scale heights (H) about disk midplane, leading to large ratios of n_i/n_e . This situation is similar to the solid curves in the two bottom panels of Figure 1, and we have confirmed that our simple four-species model well captures the η_H and η_A behaviors computed from the full chemical abundances using (3), as long as most grains are singly charged.

In the bottom panels of Figure 2, we further show the threshold field strength B_{th} (beyond which η_H changes sign) as a function of height above midplane. To guide eye, we further plot field strengths that correspond to $\beta_e = 1$ and $\beta_i = 1$ (pink), as well as field strengths that give plasma β , ratio of gas pressure to magnetic pressure, to be 1, 100 and 10^4 .

We first focus on the fiducial case with $a = 0.1\mu m$ and $f = 0.01$ (blue lines). We see that within $\sim 2H$, B_{th} is well below the $\beta_i = 1$ line, consistent with our expecta-

tions given $n_i \gg n_e$. Towards the surface, as ionization fraction approaches and then exceeds grain abundance, we see while η_H can still change sign, but at field strength well beyond $\beta_i = 1$, analogous to the top panels of Figure 1. We also note that the threshold field strength B_{th} corresponds to only modest level of magnetization, with $\beta \sim 100$ within $\pm 2H$ about midplane, which is very likely accessible in real PPDs (see next subsection).

Using different grain size and abundances yield different threshold field strengths B_{th} . Reducing dust-to-gas mass ratio by a factor of 100 to $f = 10^{-4}$ increases B_{th} by about an order of magnitude, and we see that at both 1 AU and 5 AU, field strength near or above equipartition ($\beta = 1$) is needed to have η_H change sign. This is much less likely to be achieved in PPDs, at least under standard disk models where field strength well below equipartition is sufficient to drive disk accretion at expected accretion rate (e.g., Bai 2013). On the other hand, for the same dust-to-gas mass ratio $f = 10^{-4}$, reducing the grain size further to $0.01\mu m$ yields results similar to the fiducial case. This is because smaller grains have higher total surface area/abundance at given mass, both are favorable to make charged grains dominant charge carriers.

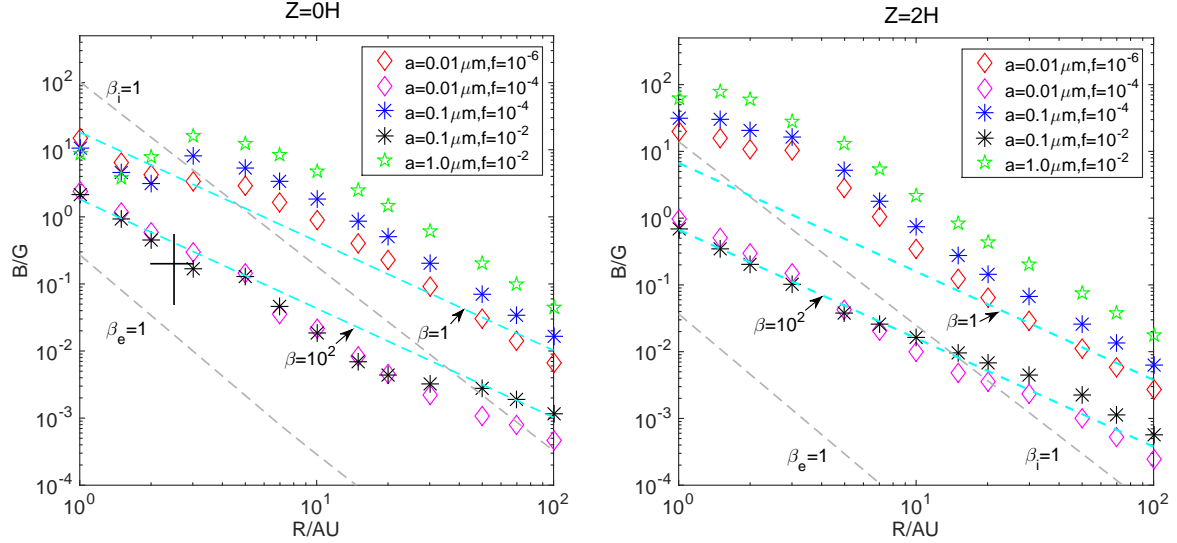


FIG. 3.— Threshold field strength B_{th} (in Gauss) beyond which the Hall coefficient changes sign, plotted as a function of disk radius R from ionization chemistry calculations at disk midplane (left) and two scale heights above midplane (right). Five combinations of grain sizes a and dust-to-gas mass ratios f are shown, as marked in the legend. To guide the eye, we also show field strengths that correspond to plasma $\beta = 1$ and 100 (black solid), as well as field strengths that give electron/ion Hall parameters $\beta_e = 1$ and $\beta_i = 1$ (grey dashed).

3.2. An Empirical Criterion on Grain Size and Abundance

Extending the discussion to a broad range of disk radii, we show in Figure 3 the threshold field strength B_{th} as a function of orbital radius R , and present the results at disk midplane ($z = 0$) and intermediate height ($z = 2H$). Moving towards larger disk radii, ionization fraction increases systematically (due to reduced density and deeper penetration of external ionization), as can be traced from Figure 2. This makes B_{th} shift up relative to the $\beta_i = 1$ line as discussed before. In the mean time, as gas density/pressure drops, field strength at fixed plasma β also shifts up relative to the $\beta_i = 1$ line, as is straightforward to show from their definitions ($B \propto \sqrt{\rho}$ v.s. $B \propto \rho$). As a result, we see from Figure 3 that line showing B_{th} as a function of R is approximately parallel the constant plasma β line over a very wide range of radii.

In Figure 3, we have considered a broad collection of grain sizes and abundances. We are particularly interested in the question of for which combinations of grain sizes and abundances can η_H change sign in the expected range of PPD magnetic field strength. We consider plasma $\beta = 100$ as a target field strength, which is easily achieved in either pure magnetorotational instability (MRI, Balbus & Hawley 1991) turbulence (e.g., Davis et al. 2010), or in more realistic studies of PPD gas dynamics (e.g., Bai & Stone 2013; Lesur et al. 2014; Bai 2014b, 2015). On the other hand, field strength above equipartition is unlikely in the disk interior. For reference, we also mark the possible field strength of the solar nebula inferred from the Semakona meteorites (Fu et al. 2014), which likely corresponds to midplane field strength at 2–3 AU during the epoch of chondrule formation. Although large uncertainties remain, field strength of up to $\beta = 100$ in an MMSN disk is reasonably consistent with the inferred nebular field strength.

From Figure 3, it is clear that small grains in large abundance is essential to make B_{th} sufficiently weak (plasma $\beta \gtrsim 100$) that can potentially be achieved in PPDs. In particular, the results from our fiducial choice of $a = 0.1 \mu\text{m}$, $f = 10^{-2}$ are very similar to those obtained with the $a = 0.01 \mu\text{m}$, $f = 10^{-4}$ case, at both $z = 0$ and $z = 2H$. This might suggest an empirical criterion where f/a^2 should be at least order unity (with a measured in μm) in order to achieve a sufficiently weak threshold field B_{th} . Note that a constant f/a^2 corresponds to a constant na where n is grain number density. Therefore, the controlling parameter is not the total grain surface area ($\propto na^2$), but lies in between total surface area and number density. We might further generalize this consideration into a distribution of grain sizes, and define

$$G \equiv \int \frac{df/da}{(a/\mu\text{m})^2} da. \quad (16)$$

Our discussions above suggest $G \gtrsim 1$ to achieve sufficiently weak B_{th} .

We note that when assuming the standard MRN size distribution for interstellar grains (Mathis et al. 1977), with $dn/da \propto a^{-3.5}$ between $a_{\text{min}} \approx 0.005 \mu\text{m}$ and $a_{\text{max}} \approx 0.25 \mu\text{m}$, we obtain $G \approx 22 \gg 1$. Therefore, while grain growth in PPDs must substantially reduces G from interstellar value, we do expect that grain-modified diffusivities is likely relevant at least in some stages of PPD evolution.

3.3. Diffusivities in the Outer Disk

Although η_H can change sign essentially at all distances, it is mainly the inner disk ($\lesssim 10$ or at most a few tens of 10 AU) that is the most relevant. Conventionally, $\beta_i > 1$ marks the dominance of AD over the Hall effect, which is achieved at lower density regions towards the outer disk. The complex dependence of η_A and η_H on field strength in the presence of abundant small

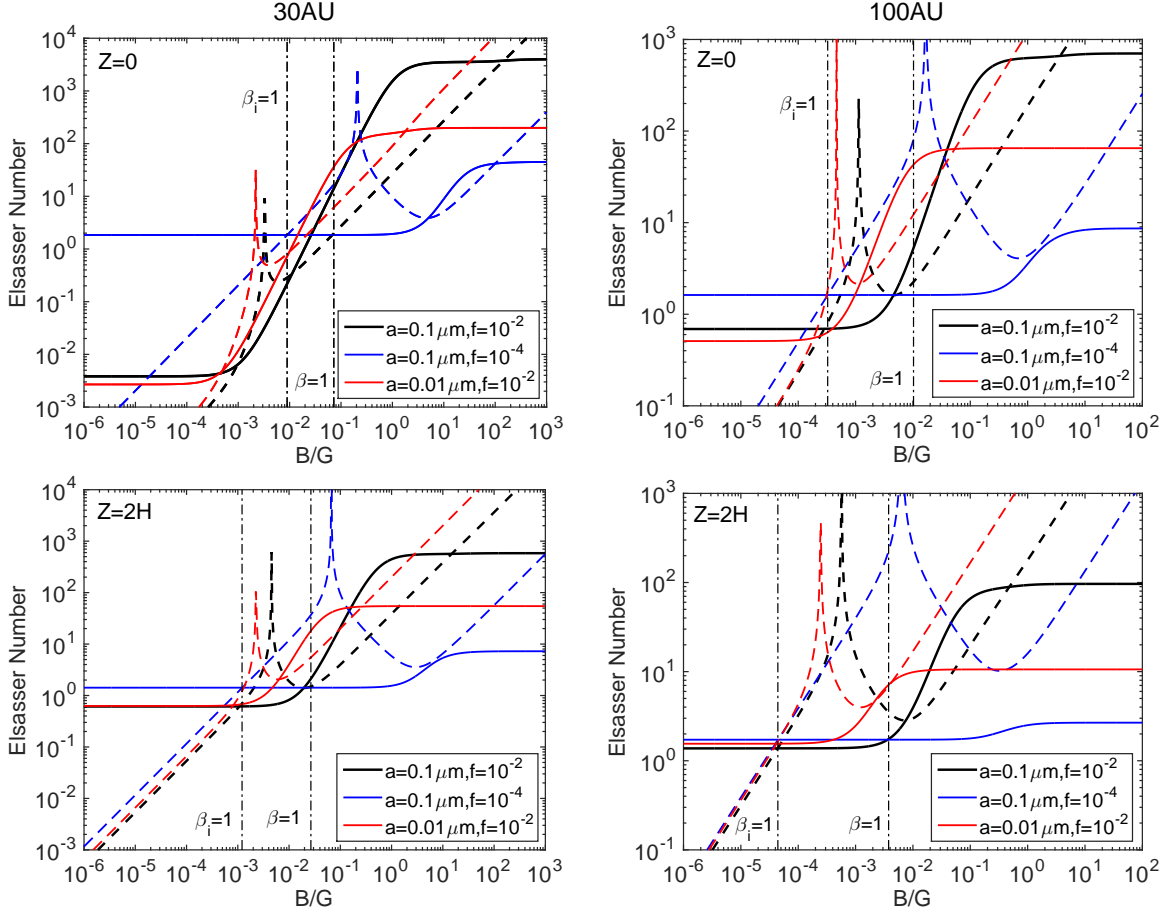


FIG. 4.— The ambipolar Elsasser number Am (solid) and Hall Elsasser number χ (dashed) as a function of field strength (in Gauss) from ionization chemistry calculations at 30 AU (left) and 100 AU (right). Top and bottom panels show the results from calculations at disk midplane, and at two scale heights above midplane, respectively. Three combinations of grain sizes a and dust-to-gas mass ratios f are shown, as marked in the legends. We also mark the field strength corresponding to plasma $\beta = 1$, as well as field strengths that give ion Hall parameters $\beta_i = 1$, in vertical dash-dotted lines.

grains complicates the situation. In Figure 4, we show the AD and Hall Elsasser numbers Am and χ as a function of magnetic field strength at 30 AU and 100 AU, at both disk midplane and intermediate height ($z = 2H$). We consider three combination of grain sizes and abundances as before and discuss the results below.

We first see that Am is constant at both weak and strong field regimes, as expected. In the presence of abundant small grains ($G \gtrsim 1$, black and red lines), the difference in Am between the two regimes can reach several orders of magnitude. In between at intermediate field strength, we have $\eta_A \approx \text{constant}$ or $Am \propto B^2$ (see also Figure 1). Therefore, AD behaves the same way as Ohmic resistivity (except for its anisotropy). These trends are the same as those discussed in B11 in the presence of tiny ($a \sim \text{nm}$) grains. If we expect field strengths in the outer PPDs correspond to plasma $\beta \sim 1 - 10^4$, then roughly speaking, the midplane region up to ~ 100 AU, and upper layer ($z = 2H$) up to ~ 30 AU would lie in this intermediate regime when $G \gtrsim 1$.

With less amount of small grains ($G \ll 1$, blue lines

in Figure 4), on the other hand, reduction of AD occurs at much stronger field. For both 30 AU and 100 AU, both at midplane and a few scale heights above, such reduction requires field strength above equipartition level, thus is unlikely to be relevant. In fact, for our choice of $a = 0.1 \mu\text{m}$ and $f = 10^{-4}$, the ionization fraction at disk midplane already exceeds grain abundance, and hence the role of grains is only minor. In this case, we see that $Am \sim 1$ is a good proxy over a wide range of disk radii and vertical locations, consistent with previous findings (Bai 2011a,b; Perez-Becker & Chiang 2011).

We also see that in the presence of abundant small grains, substantial reduction of AD towards strong field ($\beta_i > 1$) is accompanied by sign change of η_H , and the Hall effect can dominate over AD (in the conventional AD dominated regime). This is consistent features seen in Figure 1 (e.g., bottom panels). Therefore, the Hall effect may play a more important role than commonly assumed.

The AD Elsasser number Am directly controls the level of the MRI turbulence, and $Am \sim 1$ is generally consid-

TABLE 1
LIST OF ALL QUASI-1D SIMULATIONS.

R (AU)	β_0	f	Diffusivity	β_{mid}	α^{Max}	$T_{z\phi}^{z_b}$	\dot{M}_w	z_b
1	10^5	10^{-2}	full	9.50×10^3	4.00×10^{-4}	1.76×10^{-4}	2.02×10^{-5}	3.94
1	10^5	10^{-2}	simple	8.54×10^3	5.69×10^{-4}	1.95×10^{-4}	3.15×10^{-5}	3.86
1	10^5	10^{-4}	any	8.10×10^2	5.96×10^{-3}	2.67×10^{-4}	6.27×10^{-5}	4.05
1	10^4	10^{-2}	full	5.38×10^3	1.25×10^{-3}	7.46×10^{-4}	4.57×10^{-5}	3.83
1	10^4	10^{-2}	simple	4.62×10^3	2.09×10^{-3}	7.84×10^{-4}	7.22×10^{-5}	4.00
1	10^4	10^{-4}	any	4.81×10^2	1.80×10^{-2}	1.24×10^{-3}	1.30×10^{-4}	3.95
5	10^5	10^{-2}	full	5.58×10^3	2.04×10^{-4}	2.70×10^{-4}	4.97×10^{-5}	3.94
5	10^5	10^{-2}	simple	3.41×10^3	4.62×10^{-4}	3.32×10^{-4}	6.70×10^{-5}	3.91
5	10^5	10^{-4}	any	2.77×10^2	5.20×10^{-3}	4.99×10^{-4}	1.43×10^{-4}	3.91
5	10^4	10^{-2}	full	2.61×10^3	1.13×10^{-3}	1.22×10^{-3}	1.61×10^{-4}	3.83
5	10^4	10^{-2}	simple	2.08×10^3	1.88×10^{-3}	1.30×10^{-3}	1.86×10^{-4}	3.91
5	10^4	10^{-4}	any	4.61×10^2	1.75×10^{-2}	1.83×10^{-3}	2.29×10^{-4}	3.71

Note: we use grain size $a = 0.1\mu\text{m}$ for all runs, and “any” means “full” or “simple” diffusivity treatments yield same results. See Section 4.1 for more details.

ered to be sufficiently strong to substantially damp the MRI (Bai & Stone 2011; Simon et al. 2013b,a). Further introducing a modestly strong Hall term would enhance the level of turbulence if net vertical field is aligned with disk rotation $\mathbf{B}_0 \cdot \boldsymbol{\Omega} > 0$, while reduce it for opposite polarity (Sano & Stone 2002; Kunz & Lesur 2013; Bai 2015; Simon et al. 2015). The grain-modified magnetic diffusivities in the outer disk studied here may lead to two interesting effects when $G \gtrsim 1$. First, the fact that AD behaves similarly as Ohmic resistivity at intermediate field strength may lead to cycles of growth and decay of the MRI as observed in resistive MRI simulations (Simon et al. 2011). Second, the sign change of η_H means that the enhancement of the MRI by the Hall effect would occur at anti-aligned field polarity, rather than aligned polarity. These effects deserve further investigation via three-dimensional MHD simulations.

4. MHD SIMULATIONS OF THE INNER PPD

4.1. Simulation Setup and Parameters

To further study the effect of grain-modified magnetic diffusivities on PPD gas dynamics, we follow Bai (2014b) (hereafter B14) and conduct local stratified shearing-box MHD simulations that include all three non-ideal MHD terms. Note that B14 simply assumed $\eta_H \propto B$, $\eta_A \propto B^2$ in the calculations, and used a 2D diffusivity table showing the proportional coefficients as a function of density and ionization rate to compute the diffusivities. To incorporate the complex dependence of η_H and η_A on magnetic field strength, we extend the diffusivity table to 3D that explicitly accounts for this dependence.

Here we mainly focus on the inner disk region ($R < 10$ AU), where it suffices to conduct quasi-1D simulations² (as verified in Bai 2015) because the MRI is largely suppressed. The simulations use isothermal equation of state, and the simulation box extends from $-8H$ to $8H$ in z , with a resolution of 18 cells per H . We consider examples at two radii $R = 1$ AU and 5 AU, using diffusivity tables with fixed grain size $a = 0.1\mu\text{m}$ but two different abundances $f = 10^{-2}$ and 10^{-4} . An artificial boost of ionization rate beyond column densities of $\sim 0.03 \text{ g cm}^{-2}$

is included to mimic the effect of FUV ionization that brings the gas to ideal MHD regime. All simulations are conducted with net vertical magnetic field B_{z0} threading the disk, and the field strength is parameterized by plasma β_0 defined as ratio of midplane gas pressure to magnetic pressure of the net vertical field. We consider $\beta_0 = 10^4$ and 10^5 , as adopted in most previous works chosen to yield accretion rate in the expected range for the MMSN disk model. In code units, we have midplane density $\rho_{\text{mid}} = 1$, isothermal sound speed $c_s = 1$, Keplerian frequency $\Omega_K = 1$, and magnetic permeability $\mu_m = 1$.

It is well known that the effect of the Hall term depends on the polarity of background vertical field B_{z0} threading the disk (e.g., Wardle 1999; Balbus & Terquem 2001; Wardle & Salmeron 2012). Of particular interest is the case where $\mathbf{B}_0 \cdot \boldsymbol{\Omega} > 0$, or background field being aligned with rotation axis. Linear analysis as well as numerical simulations have shown that in this case, horizontal components of the magnetic field can be strongly amplified due to the Hall shear instability (HSI, Kunz 2008; Lesur et al. 2014; Bai 2014b). Because both radial and azimuthal components are amplified, Maxwell stress ($-B_R B_\phi$) is strongly enhanced which likely plays a non-negligible role in disk angular momentum transport. On the other hand, when $\mathbf{B}_0 \cdot \boldsymbol{\Omega} < 0$, the opposite occurs, and the horizontal field is reduced to close to zero near the midplane region (Bai 2014b, 2015). Because the interesting effects we have discussed in this paper operate when magnetic field gets amplified, we consider only aligned polarity $\mathbf{B}_0 \cdot \boldsymbol{\Omega} > 0$ in our simulations.

We run the simulations following the procedures of Bai (2014b). We first turn off the Hall effect during initial evolution to time $t = 120\Omega^{-1}$. Then we turn on the Hall effect and run the simulations to $t = 240\Omega^{-1}$, where steady state magnetic configuration fully saturates. In all cases, the saturated field geometry obeys “odd- z ” symmetry (e.g., Figure 9 of Bai & Stone 2013) where horizontal components of magnetic field remain the same sign across the disk, and reach maximum around disk midplane. While this symmetry is unphysical for disk wind launching, it is likely an artifact of shearing-box and here we set this issue aside³. Because magnetic

² It means that the simulation box is largely 1D in vertical, but allows for 4 cells in radial and azimuthal dimensions, which facilitates the simulations to relax to a steady state.

³ Whether a physical “even- z ” symmetry can be obtained in

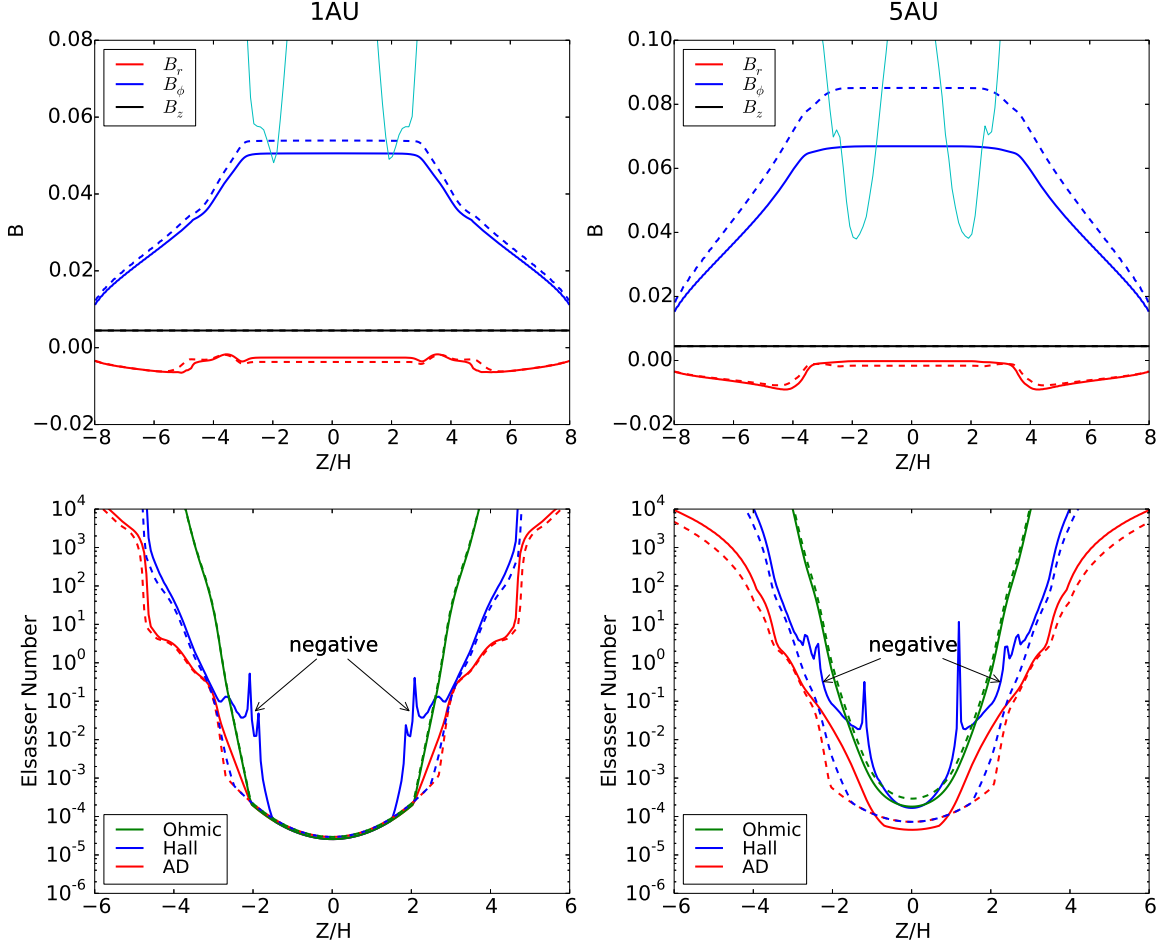


FIG. 5.— Top: vertical profiles for three components of magnetic field strength (in code units) from simulations at 1 AU (left) and 5 AU (right) in steady state, where equipartition field strength at midplane corresponds to $B = \sqrt{2}$. We have chosen grain size $a = 0.1 \mu\text{m}$ and dust-to-gas mass ratio $f = 0.01$, with weak net vertical field $\beta_0 = 10^5$. Dashed lines correspond to simulations assuming $\eta_H \propto B$ and $\eta_A \propto B^2$ in the weak field limit, while solid lines (except the cyan line) correspond to simulations using full dependence of η_H and η_A on B . Cyan solid lines mark the threshold field strength above which η_H changes sign. Bottom: vertical profiles of Ohmic, Hall and AD Elsasser numbers from simulations using full dependence of η_H and η_A on B at 1 AU (left) and 5 AU (right).

diffusivities in the disk midplane region are always excessively large at the inner disk, a diffusivity cap η_{cap} for each non-ideal MHD term is implemented to prevent prohibitively small numerical timestep. Most previous works used $\eta_{\text{cap}} \lesssim 10H^2\Omega$. We use $\eta_{\text{cap}} = 10H^2\Omega$ in the runs up to $t = 240\Omega^{-1}$ as described before, but then enlarge η_{cap} to $100H^2\Omega$ and run for another $\Delta t = 60\Omega^{-1}$, which appears sufficient for the system to relax to a new state. We do observe changes in B_R at midplane by up to 30% after enlarging the diffusivity cap, while typically the changes are within 10%, and is much smaller for midplane B_ϕ .

In parallel to simulations that take into account the full dependence of η_H , η_A on B (referred as “full”), we also

conduct simulations assuming $\eta_H \propto B$ and $\eta_A \propto B^2$, taking the proportional constants from the weak field limit of the full dependence (referred to as “simple”), and compare the difference between the two sets of runs.

Table 1 lists all our quasi-1D simulations. We also show four main simulation diagnostics at saturation: β_{mid} is the plasma β at disk midplane (based on total field strength), α^{Max} is the vertically integrated dimensionless Shakura-Sunyaev α based on Maxwell stress $\int_{-z_b}^{z_b} (-B_R B_\phi) dz / \int_{-z_b}^{z_b} \rho c_s^2 dz$, $T^{z\phi}|_{z_b}$ is proportional to the torque exerted at the wind base z_b , and $\dot{M}_w = \rho v_z$ is the mass loss rate measured at the top of the simulation box (single-sided). The wind base z_b is defined as the location where rotation transitions from sub-Keplerian to super-Keplerian (in practice, we choose it to be the first minimum of $|v_\phi - v_K|$ as one varies z from boundary towards midplane, as discussed in B14). All aspects of these diagnostic quantities have been discussed in the

shearing-box also depends on the diffusivity profiles. With $a = 0.1 \mu\text{m}$ and $f = 10^{-4}$, Bai (2014b, 2015) obtained a physical wind geometry at $R = 5 \text{ AU}$ with $\beta_0 = 10^5$. We can reproduce this result but we fail to obtain physical symmetry with $f = 10^{-2}$.

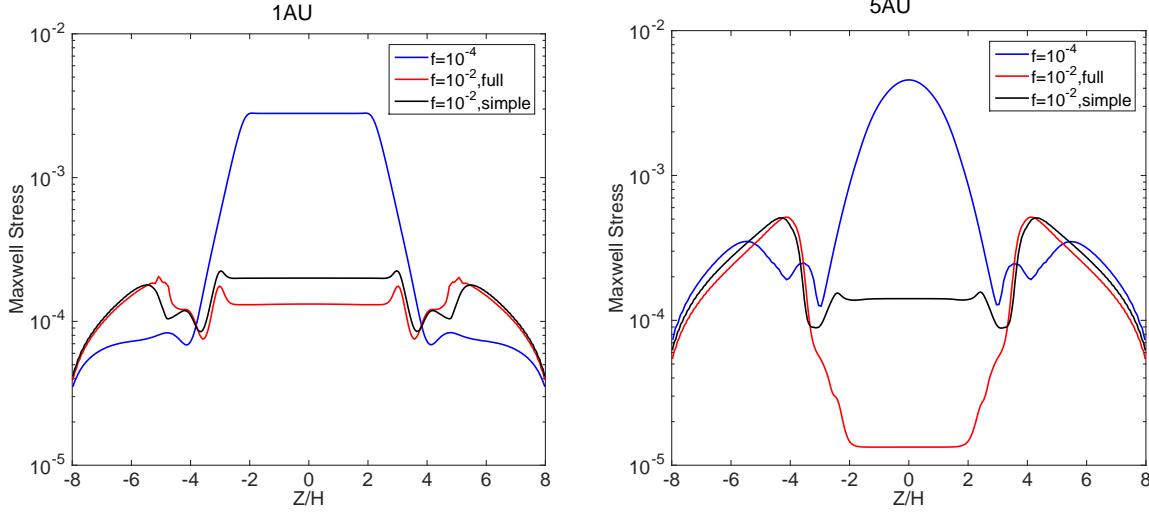


FIG. 6.— Vertical profiles of Maxwell stress from simulations at 1 AU (left) and 5 AU (right). We have chosen grain size $a = 0.1\mu\text{m}$ and dust-to-gas mass ratio $f = 10^{-4}$ (blue) and $f = 0.01$ (black and red), with weak net vertical field $\beta_0 = 10^5$. Black lines correspond to simulations assuming $\eta_H \propto B$ and $\eta_A \propto B^2$ in the weak field limit, while red lines correspond to simulations using full dependence of η_H and η_A on B .

literature, and this table mainly serves as a reference.

4.2. Simulation Results

In Figure 5, we show the simulation results with $a = 0.1\mu\text{m}$, $f = 0.01$ and $\beta_0 = 10^5$ at 1 AU and 5 AU, respectively. The top panels show the vertical profiles of magnetic field strength in code units, where plasma $\beta = 1$ at midplane corresponds to $B = \sqrt{2}$. As usual, toroidal field is the dominant component, and it maintains a relatively flat profile across the disk midplane because of excessively low ionization level there (lack of charge carriers can not support current). We also mark the threshold field strength B_{th} at which η_H changes sign, which is computed based on the diffusivity table directly. We have verified that the line shapes follow exactly the corresponding curves shown in Figure 2 in logarithmic scale. In linear scale, the minimum of B_{th} at $z = 2 - 3H$ is the most prominent feature, and we see that the saturated field strength from our simulations (dominated by toroidal field) matches closely to the minimum value of B_{th} . On the other hand, simulations assuming $\eta_H \propto B$ yield stronger field around disk midplane as a result of the HSI. This comparison clearly shows that B_{th} provides an approximate upper limit that magnetic field strength can grow, resulting in pre-matured saturation of the HSI.

The bottom panels of Figure 5 show the Elsasser number profiles for the three non-ideal MHD effects. We first see that the locations where $B < B_{\text{th}}$ in the top panels have negative Hall Elsasser number χ seen in the bottom panels. In other regions where η_H is positive, we also see that both η_H and η_A are reduced compared to the “simple” case assuming $\eta_H \propto B$ and $\eta_A \propto B^2$, which is due to a). weaker magnetic field strength and b). reduction of $|\eta_H|$ and η_A towards stronger field.

We also performed simulations with reduced grain abundance ($a = 0.1\mu\text{m}$ and $f = 10^{-4}$). In this case, however, the threshold field strength is much stronger, and we find that simulations using full diffusivity dependence on B yield identical results as assuming $\eta_H \propto B$,

$\eta_A \propto B^2$ scalings. The latter was adopted in Bai (2014b), and hence his results were unaffected. This is because with reduced grain abundance, the threshold field strength is much stronger (as seen in Figure 2), and exceeds the strength that can be attained from field amplification by the HSI.

Increasing the net vertical magnetic flux naturally leads to stronger wind, with larger wind torque and higher mass outflow rate, as listed in Table 1. Other than the wind being stronger, we find that the general phenomenologies discussed above hold exactly the same way, where field amplification by the HSI saturates at weaker field strength when full dependence of diffusivities on B is considered.

Field amplification by the HSI always weakens with increasing grain abundance as a result of enhanced resistive dissipation. This is already evident by comparing the effectively grain-free simulations of Lesur et al. (2014) and the simulations of Bai (2014b) with $a = 0.1\mu\text{m}$ and $f = 10^{-4}$, where the former showed extreme level of field amplification around the disk midplane that approach equipartition field strength, and the latter only found modest level of amplification. The trend continues when increasing dust-to-gas ratio to $f = 10^{-2}$, and assuming simple $\eta_H \propto B$, $\eta_A \propto B^2$ dependence, midplane field strength is already reduced by a factor of ~ 3 . Our simulations show that a further reduction is achieved when full dependence of diffusivities on B is considered. This further reduction in field strength is better viewed when plotting the Maxwell stress ($-B_R B_\phi$) profiles, which depends quadratically on field strength. This is shown in Figure 6, and the vertically integrated values α^{Max} are listed in Table 1.

Overall, our studies show that whether the full dependence on field strength needs to be taken into account when small grains are abundant (or effectively, $G \gtrsim 1$ defined in (16)). Reducing grain abundance leads to larger threshold field strength B_{th} , and in the mean time higher level of field amplification by the HSI. It turns

out that the former increases much faster, and the effect studied in this paper becomes essentially irrelevant when $G \ll 1$.

5. SUMMARY AND DISCUSSION

We have conducted a comprehensive study on the dependence of magnetic diffusivities on magnetic field strength in the presence of charged grains with application to PPDs. Ohmic resistivity η_O is always independent of field strength. The Hall and ambipolar diffusivities η_H and η_A obey simple asymptotic relations $\eta_H \propto B$ and $\eta_A \propto B^2$ in both weak field regime where $\beta_e < 1$, and very strong field regime where $\beta_g > 1$, while show complex dependence in between (see Figure 1). In particular, when relation (14) is satisfied (easily achieved when n_e falls below n_i due to the presence of charged grains), η_H changes sign towards strong field, accompanied by reduction of AD. The threshold field strength B_{th} beyond which η_H changes sign largely depends the ratio n_e/n_i , and is weaker when n_e/n_i is smaller (e.g., charged grains more dominant). Similarly, more abundant charged grains leads to stronger reduction of η_A/B^2 between the weak and strong field regimes.

Applying to standard MMSN model of PPDs with ionization chemistry, we find that in order for the threshold field B_{th} to be well below equipartition level, a large amount of small grains are required, as summarized in an empirical condition $G \gtrsim 1$ [defined in Equation (16)], which is applicable to a wide range of disk radii. When the same condition is satisfied, AD is also reduced substantially and may promote the action of the MRI in the outer PPDs.

We further conducted quasi-1D shearing-box simulations for inner region of PPDs including all three non-ideal MHD effects with net vertical field aligned with rotation. We show that when small grains are abundant, magnetic field amplification due to the Hall-shear instability saturates at close to the minimum value of B_{th} . Therefore, besides the fact that abundant small grains limit magnetic field growth by enhancing resistivity, they also affect the gas dynamics in a more complex way by modifying the field-strength dependence of magnetic diffusivities, especially by enabling η_H to change sign towards strong field. On the other hand, with substantial grain growth (so that $G \ll 1$), the threshold field

strength becomes too strong to be accessible via internal MHD processes in PPDs, and hence it suffices to simply adopt $\eta_H \propto B$ and $\eta_A \propto B^2$ in the weak field limit.

Our work helps clarify how the presence of grains affects ionization chemistry and magnetic diffusivities in PPDs, and hence the general disk dynamics. This is particularly relevant to the Hall effect: inclusion of the Hall effect not only makes PPD gas dynamics dependent on the polarity of net vertical magnetic field, but also leads to more sensitive dependence on grain abundance, as compared to the Hall-free case of Bai & Stone (2013). In combination with other recent studies, we can identify three regimes on the gas dynamics of inner PPDs ($\lesssim 10 - 15$ AU) depending on the grain abundance.

- Grain-free ($G \sim 0$): very strong magnetic field amplification by the HSI when $\mathbf{\Omega} \cdot \mathbf{B} > 0$ (Lesur et al. 2014; Bai 2014b), and bursty behavior at $\sim 5 - 10$ AU when $\mathbf{\Omega} \cdot \mathbf{B} < 0$ (Simon et al. 2015).
- Modest grain abundance ($G < 1$): modest magnetic field amplification by the HSI when $\mathbf{\Omega} \cdot \mathbf{B} > 0$, while horizontal field is reduced to close to zero when $\mathbf{\Omega} \cdot \mathbf{B} < 0$ (Bai 2014b, 2015).
- High grain abundance ($G \gtrsim 1$): the HSI saturates due to sign change of η_H at threshold field strength B_{th} when $\mathbf{\Omega} \cdot \mathbf{B} > 0$.

Exploration of the Hall effect in PPDs is still at an early stage. There are still pressing issues especially concerning the symmetry of disk wind, direction of magnetic flux transport, wind kinematics, etc. The complexity introduced by grains further adds to the richness of the overall subject of PPD gas dynamics. Conversely, it is well known that grain size and spatial distribution in PPDs depends on level of turbulence and global structure of the disk, and evolve with time (e.g., Birnstiel et al. 2010). The two interrelated aspects are inherent in PPD dynamics, and further call for more in-depth investigations in the future.

We thank K. Öberg for helpful advice on disk chemistry. XNB acknowledges support from Institute for Theory and Computation (ITC) at Harvard-Smithsonian Center for Astrophysics.

REFERENCES

- Bai, X.-N. 2011a, *ApJ*, 739, 50
—, 2011b, *ApJ*, 739, 51
—, 2013, *ApJ*, 772, 96
—, 2014a, *ApJ*, 791, 72
—, 2014b, *ApJ*, 791, 137
—, 2015, *ApJ*, 798, 84
Bai, X.-N., & Goodman, J. 2009, *ApJ*, 701, 377
Bai, X.-N., & Stone, J. M. 2011, *ApJ*, 736, 144
—, 2013, *ApJ*, 769, 76
Balbus, S. A., & Hawley, J. F. 1991, *ApJ*, 376, 214
Balbus, S. A., & Terquem, C. 2001, *ApJ*, 552, 235
Birnstiel, T., Dullemond, C. P., & Brauer, F. 2010, *A&A*, 513, A79+
D'Alessio, P., Calvet, N., Hartmann, L., Franco-Hernández, R., & Servín, H. 2006, *ApJ*, 638, 314
Davis, S. W., Stone, J. M., & Pessah, M. E. 2010, *ApJ*, 713, 52
Fu, R. R., Weiss, B. P., Lima, E. A., et al. 2014, *Science*, 346, 1089
Gressel, O., Turner, N. J., Nelson, R. P., & McNally, C. P. 2015, *ApJ*, 801, 84
Ilgner, M., & Nelson, R. P. 2006, *A&A*, 445, 205
Kunz, M. W. 2008, *MNRAS*, 385, 1494
Kunz, M. W., & Lesur, G. 2013, *MNRAS*, 434, 2295
Lesur, G., Kunz, M. W., & Fromang, S. 2014, *A&A*, 566, A56
Mathis, J. S., Rumpl, W., & Nordsieck, K. H. 1977, *ApJ*, 217, 425
McElroy, D., Walsh, C., Markwick, A. J., et al. 2013, *A&A*, 550, A36
Perez-Becker, D., & Chiang, E. 2011, *ApJ*, 727, 2
Salmeron, R., & Wardle, M. 2003, *MNRAS*, 345, 992
Sano, T., & Stone, J. M. 2002, *ApJ*, 577, 534
Simon, J. B., Bai, X.-N., Armitage, P. J., Stone, J. M., & Beckwith, K. 2013a, *ApJ*, 775, 73
Simon, J. B., Bai, X.-N., Stone, J. M., Armitage, P. J., & Beckwith, K. 2013b, *ApJ*, 764, 66
Simon, J. B., Hawley, J. F., & Beckwith, K. 2011, *ApJ*, 730, 94
Simon, J. B., Lesur, G., Kunz, M. W., & Armitage, P. J. 2015, *MNRAS*, 454, 1117
Turner, N. J., Fromang, S., Gammie, C., et al. 2014, *Protostars and Planets VI*, 411

Turner, N. J., Sano, T., & Dziourkevitch, N. 2007, *ApJ*, 659, 729
Wardle, M. 1999, *MNRAS*, 307, 849

—. 2007, *Ap&SS*, 311, 35
Wardle, M., & Salmeron, R. 2012, *MNRAS*, 422, 2737